Published in final edited form as:
Nanotoxicology. 2010 March 1; 4(1): 106–119. doi:10.3109/17435390903470101.

Pulmonary response after exposure to inhaled nickel hydroxide nanoparticles: short and long-term studies in mice

Patricia A. Gillespie,
[1]New York University, Department of Environmental Medicine, 57 Old Forge Rd. Tuxedo, NY, 10987, USA. Voice: (845)-731-3599, Fax: (845)-351-5472, pag286@nyu.edu

Gi Soo Kang,
[1]New York University, Department of Environmental Medicine, 57 Old Forge Rd. Tuxedo, NY, 10987, USA. Voice: (845)-731-3599, Fax: (845)-351-5472, gsk227@nyu.edu

Alison Elder,
[2]University of Rochester, Department of Environmental Medicine, 575 Elmwood Ave. Rochester, NY, 14642,USA. Voice: (585)-275-2324, Fax: (585)-256-2631, Alison_Elder@URMC.Rochester.edu

Robert Gelein,
[2]University of Rochester, Department of Environmental Medicine, 575 Elmwood Ave. Rochester, NY, 14642, USA. Voice: (585)-275-2324, Fax: (585)-256-2631, Robert_Gelein@URMC.Rochester.edu

Lu Chen,
[3]Columbia University, Department of Chemical Engineering, 500 West 120th St. New York, NY, 10027, USA. Voice: (212)-854-4453, Fax: (212)-854-3054, lc2334@columbia.edu

Andre L. Moreira,
[4]Memorial Sloan Kettering Cancer Center, Department of Pathology, 1275 York Ave. New York, NY, 10065, USA. Voice: (212)-639-5905, Fax: (212)-639-6318, moreiraa@mskcc.org

Jeffrey Koberstein,
[3]Columbia University, Department of Chemical Engineering, 500 West 120th St. New York, NY, 10027, USA. Voice: (212)-854-3120, Fax: (212)-854-3054, jk1191@columbia.edu

Kam-Meng Tchou-Wong,
[1]New York University, Department of Environmental Medicine, 57 Old Forge Rd. Tuxedo, NY, 10987, USA. Voice: (845)-731-3504, Fax: (845)-351-5472, kam-meng.tchou-wong@nyumc.org

Terry Gordon, and
[1]New York University, Department of Environmental Medicine, 57 Old Forge Rd. Tuxedo, NY, 10987, USA. Voice: (845)-731-3536, Fax: (845)-351-5472, terry.gordon@nyumc.org

Lung Chi Chen
[1]New York University, Department of Environmental Medicine, 57 Old Forge Rd. Tuxedo, NY, 10987, USA. Voice: (845)-731-3560, Fax: (845)-351-5472, lung-chi.chen@nyumc.org

Abstract

Corresponding Author: Lung Chi Chen, PhD, Dept. of Environmental Medicine, New York University, 57 Old Forge Rd. Tuxedo, NY 10987, USA. Fax: 845 351 5472. lung-chi.chen@nyumc.org.

Declaration of Interest
The authors report no con!icts of interest. The authors alone are responsible for the content and writing of the paper.

Short and long-term pulmonary response to inhaled nickel hydroxide nanoparticles (nano-$Ni(OH)_2$, CMD = 40 nm) in C57BL/6 mice was assessed using a whole body exposure system. For short-term studies mice were exposed for 4 h to nominal concentrations of 100, 500, and 1000 mg/m^3. For long-term studies mice were exposed for 5 h/d, 5 d/w, for up to 5 months (m) to a nominal concentration of 100 mg/m^3. Particle morphology, size distribution, chemical composition, solubility, and intrinsic oxidative capacity were determined. Markers of lung injury and inflammation in bronchoalveolar lavage fluid (BALF); histopathology; and lung tissue elemental nickel content and mRNA changes in macrophage inflammatory protein-2 (Mip-2), chemokine ligand 2 (Ccl2), interleukin 1-alpha (Il-1α), and tumor necrosis factor-alpha (Tnf-α) were assessed. Dose-related changes in BALF analyses were observed 24 h after short-term studies while significant changes were noted after 3 m and/or 5 m of exposure (24 h). Nickel content was detected in lung tissue, Ccl2 was most pronouncedly expressed, and histological changes were noted after 5 m of exposure. Collectively, data illustrates nano-$Ni(OH)_2$ can induce inflammatory responses in C57BL/6 mice.

Keywords

Nickel; nanoparticles; inhalation; lung; pulmonary response

Introduction

Numerous forms of nanomaterials are currently being used to advance the field of nanotechnology. Included are nanoparticles (NPs, particle diameter <100 nm), which have gained interest for use in industrial applications due to their catalytic, optical, and electronic properties (Gornostaeva et al., 2008; Fangli et al., 2002). With an estimated economic output exceeding $1 trillion by 2015, there are legitimate concerns about the potential adverse health effects that these NPs may cause (Maynard 2007; Roco and Bainbridge 2001). Inhalation is likely a major route of occupational or accidental exposure due to the probability that NPs will become airborne during different phases of use (e.g. synthesis, production, distribution, and disposal). A lung deposition model developed by the International Commission of Radiological Protection (ICRP) predicted that inhaled NPs can efficiently deposit in all regions of the respiratory tract. As compared to larger particles, NPs have higher predicted fractional deposition in the nose and alveolar region of lungs, enhancing the risk for adverse pulmonary effects to occur (ICRP, 1994). In addition, it has been demonstrated that compared to larger particles of similar composition, NPs are more inflammatory and cytotoxic (Lewinski et al. 2008; Oberdorster et al. 1994). Conclusions were drawn that the observed effects were not only due to the small size of these particles, but also attributable to their unique physical and chemical properties (e.g. solubility, surface characteristics, and ability to penetrate biological membranes).

The aim of this study was to assess the pulmonary response to inhaled nickel nanoparticles in a mouse model. Short-term studies (single 4 h exposure) were conducted first in order to gain preliminary insight about potential pulmonary toxicity. Dose-response relationships were established and used to determine the dose for repeated exposures. Using the established dose of 100 $\mu g/m^3$, long-term studies (1 week [w], 3 months [m] or 5 m of daily exposure) were conducted to profile pulmonary changes induced by repeated exposure to inhaled nickel nanoparticles. Commercially, nickel is a valuable commodity with many industrial applications. Characterization of the chemical composition revealed our nanoparticles to be nickel hydroxide (nano-$Ni(OH)_2$) which has gained interests in a number of industrial uses, especially those involving electrochemical processes (Fetcenko et al., 2007; Vidotti et al, 2008). Experimental data shows that when nano-$Ni(OH)_2$ are added to the cathodes of alkaline batteries, an enhanced discharge specific capacity results (Boyer et

al., 2004; Xiao-yan and Jian-cheng 2007). This is an attractive property because it translates into longer battery output. However, despite the growing interest in nano-$Ni(OH)_2$, there has been no evaluation to date on the potential health effects that may occur following inhalation exposure.

In this study, we exposed mice via a whole body inhalation system to laboratory generated nano-$Ni(OH)_2$ at mass concentrations lower than the current Occupational Safety and Health Administration permissible exposure limit (OSHA PEL, 1 mg Ni/m^3). Because characterizing NPs under investigation is of utmost importance, a variety of analytical techniques were employed to describe our tested particles. These methods included: scanning mobility particle sizing (SMPS) to measure airborne size distributions; transmission electron microscopy (TEM) to investigate particle morphology; X-ray photoelectron spectroscopy (XPS) and X-ray fluorescence spectroscopy (XRF) to determine and confirm chemical speciation; and dialysis to measure the dissolution of our Ni NPs in simulated lung lining fluid and alveolar macrophage milieu. In addition, we determined the amount of nickel present in lungs.

The toxicological profiles of other nickel-containing materials and metal-based NPs have demonstrated adverse effects marked by inflammation following inhalation exposures. Benson and colleagues have reported repeatedly on soluble and insoluble nickel compounds inflammatory effects in the lungs (e.g. nickel sulfate, subsulfide, and oxide) (Benson et al., 1995); and others have demonstrated that metal nanoparticles like titanium and silver are also able to induce inflammatory related responses in the lung (Grassian et al., 2007; Jae-Hyuck et al., 2008). Consequently, we assessed this response paradigm. Markers of inflammation and lung injury were measured in bronchoalveolar lavage fluid (BALF) and gene expression analyses of several cytokines and chemokines involved in inflammatory processes were assessed in lung tissues. A histological examination was performed after long-term studies in order to evaluate the extent of inflammation and injury in the lungs following repeated exposures. Since unchecked oxidative stress can lead to inflammation, the intrinsic oxidative capacity of the Ni NPs was also measured using a cell-free system.

Materials and Methods

Animals

Male C57BL/6 mice (12 weeks old, body weight 20–25 g) were obtained from Taconic Farms (Germantown, NY) and housed in our AAALAC accredited housing facility in Tuxedo, NY. Animals were kept on normal 12h light/ dark cycles and received food and water *ad libitum*, except during exposure. After a two week acclimation period, mice were exposed in whole body inhalation chambers to either filtered air or nano-$Ni(OH)_2$. Details about the exposure chambers have been previously described elsewhere (Maciejczyk et al., 2005). All procedures were conducted in compliance with New York University's guidelines for ethical animal research.

Short-term studies—Animals were exposed for 4 h to low, mid, or high mass concentrations of: 103.2, 565.0, and 1204.0 $\mu g/m^3$ (65.4, 358.2, and 763.3 $\mu g\ Ni/m^3$), respectively. Animals were euthanized with an overdose of sodium pentobarbital (150–200 mg/kg) via an intraperitoneal injection at 0.5 or 24 h post-exposure in order to determine lung deposition and initial clearance of nickel (n = 4/group) Additional groups of animals exposed to the low and high concentrations were euthanized at 48 h post-exposure (n = 3/ group). Since only 25 mg of lavaged lung tissue was needed for RNA extraction (harvested from the lower region of one lobe) and recovered BALF for the biochemical assays, one cohort of animals was used for dosimetry and effects studies. Control mice were treated in a similar manner but were only sacrificed 24 h post-exposure (n = 3).

Long-term studies—Animals were exposed for 5 h/d, 5 d/w, for 1 w, 3 m, or 5 m to nano-$Ni(OH)_2$ at average chamber concentrations of 124.0, 129.3, and 124.5 μg/m^3 (78.6, 82.0, 79.0 μg Ni/m^3), respectively. Lung nickel content and biological response markers were assessed 24 h after the last exposure. Mice for dosimetry and biological assays were treated in the same manner as described above for nickel-exposed and control groups (n = 3–4, Ni-exposed and n = 3, control). The extent of lung inflammation and injury were also examined histologically following 5m of exposure using fixed tissue samples from a separate cohort of animals (n = 4/group).

Generation of Nano-$Ni(OH)_2$ and the exposure system

Particles were produced by opposing metallic nickel electrodes (99.995% purity, ESPI, Ashland, OR) in an ultra pure argon chamber using a Palas® GmbH arc furnace (Model GFG-1000, Karlsruhe, Germany). Ultra pure oxygen was added to filtered dilution air in order to keep the exposure atmosphere at 20% oxygen. Animals were exposed to nano-$Ni(OH)_2$ in a whole body exposure chamber (Figure 1). Control animals were housed in a similar fashion but only received filtered air. Wipe tests of chamber surfaces showed little surface deposition of Ni nanoparticles and, therefore, oral dose was expected to be negligible as compared to inhaled dose.

Characterization of nano-$Ni(OH)_2$

Particle size distribution and number concentrations were determined using instrumentation (TSI, St. Paul, MN; consisting of model 3071 electrostatic classifier and model 3010 condensation particle counter) which sampled the exposure atmosphere just upstream of the animal exposure chamber. Particles were also collected from the same location on 0.5% formvar coated 400 mesh copper grids (Ted Pella Inc., Redding, CA) for analysis using TEM (CM12 model, Philips). The chemical speciation was analyzed using XPS on particle-laden Teflon filters. XPS spectra were recorded with a PHI 5500 spectrometer (Physical Electronics, Chanhassen, MN) operated at 15 kV and 23.3 mA. No beam damage was induced on the sample surface. A nonlinear least-squared curve fitting was completed using RBD software, AugerScan 3, with a mixed Gaussian/Lorentzian function. Exposure total mass concentrations were determined by gravimetric analysis and nickel mass concentrations by XRF analysis (model EX-6600-AF, Jordan Valley, Austin, TX; and spectral software XRF2000v3.1 U.S.EPA and ManTech Environmental Technology, Inc., Research Triangle Park, NC) of Teflon filters (37 mm diameter, 0.2 μm pore, Gelman Sciences, Ann Arbor, MI). The filters were kept in a temperature and humidity controlled room (21 ± 0.5°C and 40 ± 5%, respectively) and weighed before and after sampling using a microbalance (model MT5, Mettler Toledo, Highstown, NJ). Nano-$Ni(OH)_2$ mass concentrations and size from all exposures are summarized in Table I.

The solubility of nano-$Ni(OH)_2$ was evaluated by measuring the dissolution of particles in a flow-through dialysis system developed by Potter and Mattson (1991) and described in Elder et al. (2006), with physiologic buffers that mimicked lung epithelial lining fluid (pH 7.4) and the phagolysosome of alveolar macrophages (pH 4.5). The measurements were made at 37°C and at room temperature (~23°C). The molecular weight cut-off of the dialysis membrane was 3500 daltons (effective pore size ~2 nm; thickness, 25 μm) and was made of regenerated cellulose (Molecular/Por cellulose ester asymmetric membrane; Spectrum Laboratories, Inc., Rancho Dominguez, CA). Dialysates were collected over a period of 29 h in order to obtain stable rate constants. Dialysates and the membranes themselves were analyzed for Ni content using direct current plasma atomic emission spectroscopy. The membranes retained very little of the Ni (average of 0.003% of starting material at pH 7.4; 0.166% at pH 4.5 after 29 h).

The intrinsic oxidative capacity of nano-$Ni(OH)_2$ and nickel sulfate ($NiSO_4 \cdot 6H_2O$) (Alfa Aesar, Ward Hill, MA) were measured using a fluorescein derivative (2',7'-dichlorodihydrofluorescein diacetate, DCFH-DA; Invitrogen, Carlsbad, CA) reporter system, as modified from Venkatachari et al. (2005). In brief, the dye was deacetylated with 0.01 N NaOH and then converted to its fluorescent form (DCF) by hydrogen peroxide (H_2O_2) or oxidizing species generated by NPs. Horseradish peroxidase (HRP) was added to the solution in order to enhance the oxidation. Particle activity was compared to that of H_2O_2 (standards from 0–1290 nM) and expressed as H_2O_2 equivalents. The presence of HRP alone did not induce an increase in fluorescence (≤7 nM equivalents). If HRP is removed from the assay system, no H_2O_2-induced fluorescence is detected; likewise, nano-$Ni(OH)_2$ induced (6 μg Ni) DCF fluorescence is also undetectable when HRP is absent.

BALF assays

The trachea was cannulated and the lungs lavaged twice with 1.2 ml of phosphate buffered saline without calcium and magnesium (PBS, Invitrogen, Carlsbad, CA). Harvested fluid from short-term studies was used to examine cell differential and total protein levels. For cell differentials, an aliquot of lavage fluid was prepared using cytospin (Shandon, Southern Products, UK) with subsequent Hemacolor® staining (EM Science, Gibbstown, NJ). Neutrophil population was enumerated by counting 100 total cells. The remaining lavage fluid was centrifuged at 400 g for 10 min and the collected supernatant was analyzed for total protein levels using bovine serum albumin as a standard (BioRad, Hercules, CA). For long-term studies BALF was harvested as described for the short-term studies but, additional parameters were investigated. Macrophage, neutrophil, and lymphocytes populations were enumerated. In addition to determining total protein levels, cell free aliquots were also analyzed for N-acetyl-glucosaminidase (Boehringer Mannheim, Indianapolis, IN). This assay was modified for use on a Konelab Arena 30 clinical analyzer (Thermo Chemical Lab Systems, Espoo Finland). BALF samples were also analyzed for chemokine (C-C motif) ligand 2 (CCL2, also known as MCP-1) by Enzyme-Linked Immunoassays using a commercially available kit (R&D Systems, Minneapolis, MN). Duplicate samples were analyzed for all BALF assays.

Lung tissue nickel content determination

Lungs were lavaged and removed from animals for nickel elemental analyses. Individual lungs were weighed and wet ashed in Teflon beakers using optima grade nitric acid (HNO_3) and hydrogen peroxide (H_2O_2) (Fisher Scientific, Pittsburgh, PA). Following digestion, samples were collected in 15 mL conical tubes with a final volume of 2 mL. Prior to analysis, analytes were diluted using 18 MΩ deionized water to 0.2%. The amount of nickel present in each sample was determined with graphite furnace atomic absorption spectroscopy (GF95, Thermo Scientific, Waltham, MA) using a 5-point calibration curve constructed from certified nickel reference standards (Fisher Scientific, Pittsburgh, PA).

Quantitative RT-PCR

Approximately 25 mg of lavaged lung tissue from the lower left lobe was harvested 24 h post-exposure and stored in RNA*later*® Solution (Ambion, Austin, TX) at −20°C until further processing. Using RNeasy mini kits (Qiagen, Valencia, CA), total RNA was extracted and treated for genomic DNA contamination. The quality and concentration was determined using a Nanodrop 1000 spectrometer (Thermo Fisher Scientific, Wilmington, DE). Using High Capacity cDNA Reverse Transcription Kits (Applied Biosystems, Foster City, CA) and following the provided manufacturer's protocol, total RNA was reverse transcribed into cDNA. To quantify relative mRNA levels of selected genes: macrophage inflammatory protein-2 (Mip-2), Ccl2, interleukin 1-alpha (Il-1α), and tumor necrosis factor-alpha (Tnf-α), real-time polymerase chain reaction (PCR) was performed on an Applied

Biosystems 7300 Real-Time PCR instrument (Applied Biosystems, Foster City, CA), under the following conditions: 10 min at 95°C followed by 40 cycles at 95°C and 60°C (15 sec and 1 min, respectively). With primer/probe sets from TaqMan® Gene Expression Assays, the forward and reverse primers were specific to each gene and synthesized by Applied Biosystems from the following mRNA reference sequences: Il-1α (NM_010554.4); Tnf-α (NM_013693.2); Mip-2 (NM_009140.2); and Ccl2 (NM_011333.3). Relative expression levels were established using the comparative C_T method outlined in the ABI technical guide for performing real time quantitative PCR (Applied Bioystems). All expression levels were normalized to the housekeeping gene, hypoxanthine phosphoribosyltransferase [Hprt-1, reference sequence (NM_013556.2)], and reported as a relative fold change over control ± standard deviation (SD).

Lung histology

Lung tissues were fixed 24 h after 5m of exposure via transcardial whole body perfusion using 4% paraformaldehyde/ 4% sucrose in phosphate buffer saline (pH 7.4). Following fixation, lung tissue samples were removed, briefly washed with PBS and embedded in paraffin. Serial sections of 5 μm thickness were stained with hematoxylin-eosin (H&E) and examined by a board certified pathologist (ALM).

Statistical analyses

One-way analysis of variance followed by Bonferroni's multiple comparisons post-hoc test or an unpaired Student's t-test was used to evaluate treatment-related effects. A p-value equal to 0.05 was considered as the threshold for statistically significant differences between groups. Data were analyzed using Graphpad Prism Software (5^{th} Edition, La Jolla, California) and are expressed as mean ± standard error of the mean (SEM), unless otherwise noted.

Results

Particle characterization

The CMD of the generated nano-$Ni(OH)_2$ particles was approximately 40 nm, with an overall average geometric standard deviation of 1.50 for all studies (Table 1). The particle size distribution determined by SMPS agreed well with TEM images, which also revealed 40 nm NPs that were agglomerates of approximately 5 nm primary particles (Figure 2A and Figure 3). The generated particles were analyzed by XPS, and the curve fitting for the Ni 2p spectrum is shown in Figure 4. There are two main peaks within the Ni 2p region: 2p3/2 and 2p1/2; and for each main peak there are two shake-up satellite peaks: S1 and S2. The peak positions and area percentages from the curve fitting are shown in Table II. To determine the chemical composition, we compared the Ni 2p peaks of our generated particles with those of other common nickel compounds. As can be seen in Table III, the XPS parameters of the generated particles are very close to that of a $Ni(OH)_2$ signature, indicating it to be the most likely chemical species of the NP generated in our system. XRF analysis results were also consistent with $Ni(OH)_2$, showing 62.3 ± 2.5% of total particle mass was attributable to Ni (molecular weight ratio of nickel to $Ni(OH)_2$: approximately 59/93=63.4%). XRF analysis was also used to check impurities in generated particles, and the results revealed all 33 tested elements to be below the lower limit of detection (data not shown).

Dissolution rates were assessed using dialysis in physiological buffers that simulated lung epithelial lining fluid and macrophage phagolysosomal conditions. Cumulative fractional dissolution in these buffers was determined through 29 h (Figure 5A, B). By 24 h, 85.6% and 95.9% of the starting material was dissolved at pH 7.4 and 4.5, respectively. Dissolution rates were lower at room temperature than at 37 °C, as expected. It is noted that data

reported for 14–22 h are estimates from a single aliquot that was collected overnight and from the rate constant calculated from the first 13 measurements.

The NP oxidative capacity measurements showed that the reactivity of the nano-$Ni(OH)_2$ exceeded the highest standard (1290 nM H_2O_2) between 1.59 and 3.16 μg of Ni by mass in solution. As a comparison, a soluble Ni compound ($NiSO_4 \cdot 6H_2O$) was also used in this system, in which samples up to 6.32 μg of Ni by mass did not produce appreciable dye oxidation (range: <detection limit to 25 nM H_2O_2 equivalents) (Table IV).

Lung nickel content

To estimate initial lung burden of nano-$Ni(OH)_2$, an inhaled dose was first calculated for all short-term exposure concentrations. This calculation was based on the assumption that 100% of the dose was deposited throughout the lung and from mouse tidal volume, breathing frequency, and exposure concentration and duration data (*Biology of the Laboratory Mouse*; Bernstein, 1975). Using the calculated inhaled dose, total lung deposition rates of 17.1, 24.1, and 21.6% were determined at 0.5 h post-exposure for mice exposed to low, mid, and high nano-$Ni(OH)_2$ concentrations, respectively. Clearance was assessed by examining the Ni tissue content at 24 h post-exposure. It was determined that 69.9, 47.4, and 46.0% of the initial (0.5 h) deposited nickel had cleared, most likely via the mucociliary escalator (Chen and Schlesinger, 1983) from lungs exposed to low, mid, and high nano-$Ni(OH)_2$ concentrations, respectively. In animals exposed to the low and high concentrations, an additional 8.9 and 17.4% of the deposited Ni had further cleared from the lung tissue within 48 h post-exposure, respectively (Table V). TEM images of BALF taken from a single mouse exposed to the high nano-$Ni(OH)_2$ concentration, 0.5 h post-exposure, showed electron dense nickel particles that appeared to be more dispersed than the particles observed from the exposure atmosphere and displayed smaller aggregates of the primary particles (Figure 2B). Following repeated exposures, nickel accumulation was assessed 24 h after the last exposure and, as shown in Table VI, total lung nickel content increased with exposure duration.

Biological Response

For short-term studies, BALF was collected 24 h post-exposure to assess PMN infiltration and protein leakage into the lungs. In mice exposed for one day to low, mid, and high nano-$Ni(OH)_2$, 1%, 7%, and 28% of the total cell population was comprised of PMNs, respectively (Figure 6A). Compared to the control mice, only the mid and high concentration data indicated a statistically significant response; protein levels in BALF reflected this same trend (Figure 6B). Given this data, a nominal dose of 100 $\mu g/m^3$ was chosen for repeated exposures because it was the least toxic of the tested concentrations. Table VII shows time-related changes in BALF parameters. In mice repeatedly exposed to nano-$Ni(OH)_2$, total neutrophil and lymphocyte populations were significantly increased after 3 m and 5 m of exposure. At these same time periods, protein levels were significantly increased as well. Interestingly, the neutrophil and protein levels were lower at 5 m compared to 3 m, possibly suggesting an adaptive response. Since nickel accumulation appeared to increase in a linear fashion, the activity of N-acetyl-glucosaminidase (NAG) was also measured after 1w and 5m of exposure as a marker of phagocytosis by alveolar macrophages. Data was only significant for NAG after 5 m of exposure.

Inflammatory cytokine and chemokine (Il-1α, Tnf-α, Mip-2, and Ccl2) mRNA expression levels in lavaged lung tissue were also measured 24 h post-exposure (Figure 7A, 7B). Following short-term exposures, significant induction of Ccl2 and Mip-2 was detected in the lungs of mice exposed to mid and high nano-$Ni(OH)_2$. While Il-1α was not significantly up-regulated at any of the exposure concentrations, Tnf-α expression was increased at the high

concentration. Variable mRNA expression was observed after repeated exposures to 100 μg/m^3 of nano-$Ni(OH)_2$. Significant up-regulation of Ccl2 was observed following 3 m and 5 m of exposure. Induction of Mip-2 and Tnf-α was observed after 3m of exposure, while Il-1α was only significantly up-regulated following 5m of exposure. Of the genes assessed, Ccl2 showed the most pronounced increase in expression and, consequently, protein levels for this chemokine was measured in BALF. As indicated in Table VII, MCP-1 was significantly elevated after 3 and 5 m of exposure.

Histology—The lungs of mice exposed to nano-$Ni(OH)_2$ showed mild and focal inflammatory infiltrate in the pulmonary parenchyma following a 5m exposure. The inflammation was mainly observed around blood vessels and terminal ducts. The infiltrate was predominantly composed of small, mature-appearing lymphocytes (Figure 8). The remainder of the pulmonary parenchyma appeared normal.

Discussion

The objectives of this study were to characterize aerosolized nano-$Ni(OH)_2$ and to assess biological responses resulting from short and long-term inhalation exposures in mice. The majority of published works investigating pulmonary effects of nanoparticles *in vivo* have been conducted utilizing routes with limited biological relevance (e.g. intratracheal instillation, intraperitoneal injection, and intrapharyngeal aspiration). We used here a study design with the greatest relevance toward human exposures, namely aerosol inhalation. All exposures were conducted using a whole body exposure system, which comes with inherent advantages: uniform distribution of the inhaled particles to a large group of animals; reduced animal stress due to minimal restraint; and a design that mimics human inhalation scenarios (Bakand et al., 2005; Dorato, 1990). To address the concerns that dermal and gastrointestinal exposure via particle deposition on the animals' fur and animal grooming activities in a whole body exposure system (Phalen, 1996) we performed wipe tests on chamber surfaces and found that there was little surface deposition of nano-$Ni(OH)_2$ (below the detection limit of XRF) suggesting that demal and oral dose are negligible compared to inhaled dose. In addition, all concentrations used in this study were below the current OSHA PEL (1 mg Ni/m^3),

Data in Table 1 indicates that the CMD of our NPs were approximately 40 nm. Based on ICRP deposition models, these particles most likely deposited throughout the lungs, with more deposition in the alveolar region as compared to other regions. It has been established that initial clearance of insoluble particles in the conducting airways occurs within the first 24 h post-exposure via the mucociliary escalator (Hofmann & Asgharian, 2003). In the lower airways, clearance usually occurs via phagocytosis by resident and infiltrating macrophages over a period of one to two weeks or through particle dissolution (Schlesinger, 1985). The efficiency of this alveolar clearance mechanism in regard to NPs is unclear since it has been shown that they are not efficiently engulfed as singlets by macrophages (Geiser et al., 2008). For partially soluble NPs in biological fluids, such as $Ni(OH)_2$ used in this study, clearance mechanisms are even more complex. An additional factor, as shown in Figure 2B, is that the lung lining fluid appeared to promote the dispersion of the nano-$Ni(OH)_2$ agglomerates; furthermore, results obtained from NAG measurements in BALF suggest phagocytic activity was increased following 5 m of exposure.

We have determined the clearance rates of nano-$Ni(OH)_2$ as nickel following acute exposures and the data indicate that for all tested concentrations, the clearance half-time is approximately one day (Table V). Using a mathematical model, Hsieh et al., (1999) determined nickel deposition of several compounds in the mouse lung based on previously reported experimental data. A clearance half-time of 63 days for nickel subsulfide (particle

diameter [dp] = 2.5 and 2.2 μm), 82 days for nickel oxide (dp= 2.8, 2.3, and 1.9 μm) and 1.6 h for soluble nickel sulfate (dp= 2.3 μm) was calculated. Differences in exposure durations (ranging from 13 weeks to 2 years), concentrations (ranging from 0.2 to 12.6 mg/m^3), and particle size must be taken into account and may explain dissimilarities in clearance half-times. However, considering these data, it appears that our nano-$Ni(OH)_2$ have clearance rates most similar to soluble nickel sulfate. Studies have shown that as the size of particles decreases, the surface chemistry changes (i.e. increased surface area and energy), which can result in increased solubility (Hammond et al., 2007;Sergeev, 2006).

Non-equilibrium solubility tests of nano-$Ni(OH)_2$ using physiological buffers revealed dissolution rates of 86% at neutral pH and ~100% at pH 4.5 in 24 h. Kasprazak et al. (1983) calculated a solubility rate of 50% at 78 days for micrometer sized $Ni(OH)_2$ in neutral pH physiological buffer (37°C) using a liquid scintillation technique. While direct comparison is not practical given the differences in the methodologies (e.g. assay method and equilibrium conditions), the data still highlights that our nano-$Ni(OH)_2$ dissolved more rapidly, likely a result of the aforementioned increase in solubility as particle size decreases. Since solubility is a key factor in clearance and our data shows that following single exposures to nano-$Ni(OH)_2$ there is continuous clearance over two days, it was important for us to determine whether significant amounts of Ni could accumulate in lung tissue after repeated exposures. Results from our long-term studies show that after 1w, 3m and 5m of exposure, Ni does in fact accumulate in lung tissue in a time-dependent manner (Table VI).

The reactivity (oxidative capacity) of the NP can also impact dissolution and biological response (e.g. oxidative stress induction). Cell-free tests of dye oxidation by the nano-$Ni(OH)_2$ demonstrated that maximal responses were reached with low μg amounts of Ni (Table IV). At 1 μg, nano-$Ni(OH)_2$ had an activity that was equivalent to the dye oxidation caused by 613 nM H_2O_2 (interpolated from data in Table IV). Interestingly, when soluble $NiSO_4{\cdot}6H_2O$ was tested using the same method, there was no significant ROS production detected (up to ~6 μg of Ni). While this method provides information about oxidant capacity, it lacks specificity in terms of the reactive species that induce DCF fluorescence. Nevertheless, the data demonstrate that solubility and other characteristics, like particle surface reactivity, are important to consider when evaluating mechanisms of toxicity.

It has been shown that particles and dissolved ions interact with cellular components via distinct mechanisms that influence their potential toxic fates (Lu et al., 2005). *In vitro* studies illustrate that toxic effects of nickel compounds are ultimately determined by the concentration of bioavailable nickel ions, especially intracellularly (Fletcher et al., 1994; Ke et al., 2007). While soluble particle fractions have greater potential to gain entrance into the blood circulation, particle transport inside of the cell is limited by: rates of solubization and clearance; interactions with extracellular proteins; affinity for ion transporters like the divalent metal ion transporter (DMT1); endocytosis; and transmembrane passive diffusion (Chen et al., 2005; Davidson et al., 2005; Oller et al., 2002). All of these are dynamic interactions, adding to the complexity of toxicological response mechanisms. Benson et al. (1986) demonstrated that in acute instillation studies in rats, the dissolution of nickel compounds was an important factor for observed effects with the following ranked respiratory toxicities: nickel subsulfide (Ni_3S_2) ~ nickel chloride ($NiCl_2$) ~ nickel sulfate ($NiSO_4$) >> nickel oxide. Given the solubility rate of our nano-$Ni(OH)_2$, we expected the toxicities to be similar to that of Ni_3S_2, $NiCl_2$, and/or $NiSO_4$. However, particle size, a very important parameter, was not reported in the Benson et al. (1986) study, so direct comparisons are not possible.

Lung inflammation has been identified as a major concern for inhalation exposure of NPs. In BALF collected 24 h post-exposure, we found statistically significant increases in PMNs

and total protein levels after single exposures to mid and high concentrations. And after 3 m and 5 m of repeated exposures to 100 μg/m^3 of nano-$Ni(OH)_2$ significant increases were also observed for these two markers but in addition to linear increases in lymphocyte populations and MCP-1 protein levels.

It is well known that cytokines and chemokines are involved in the activation and recruitment of cells to sites of inflammation and assist in the progression of inflammatory events (Feghali and Wright, 1997). In lung tissue, we quantified Il-1α, Tnf-α, Mip-2, and Ccl2 mRNA expression by real-time RT-PCR. Studies have shown that Il-1α and Tnf-α are key cytokines involved in the development and progression of inflammation and Ccl2 and Mip-2 are mediators involved in the migration of leukocytes to sites of inflammation and injury (Driscoll et al., 1997; Feghali and Wright, 1997). *In vitro*, it has been demonstrated that while Mip-2 and Ccl2 are both involved in the aforementioned events, Mip-2 is the more potent inducer of neutrophil migration as compared to Ccl2, which, to a greater extent, induces the migration of monocytes/macrophages (Driscoll et al., 1995; Fahey et al., 1992; Fulton et al., 2002). The up-regulation of Ccl2 and Mip-2 at the mid and high concentrations was significant and consistent with our observed BALF analyses of PMN infiltration. Comparing Ccl2 and Mip-2 mRNA expression at the mid and high exposure concentrations, Ccl2 showed a more pronounced up-regulation in mouse lungs (Figure 7A). A recent study by Maus et al. (2003) demonstrated crosstalk between monocytes/ macrophages and PMN mediated by significant amounts of secreted macrophage related chemokines (namely Ccl2). This cell to cell communication was shown to facilitate a strong influx of PMN to sites of inflammation. These findings may explain our predominance of Ccl2 expression along with sustained elevations in neutrophils (Table VII).

In our long-term studies, we found significant increases in Mip-2 after 1 w and 3 m of exposure; and Ccl2 was significantly up-regulated after 3m and 5m of exposure (Figure 7B). In addition, leukocyte populations were significantly different than controls following 3 m and 5 m of exposure with the highest PMN percentage observed after 3m and lymphocyte percentage following 5 m of exposure (Table VII). These results are consistent with the traditionally described inflammatory line of defense stating that PMN appear first, followed by slow progressing macrophages and lymphocytes. Histological evaluation after 5m of exposure corroborates these findings with observed mild inflammatory infiltrates in the pulmonary parenchyma which were mostly comprised of lymphocytes (Figure 8). However, the findings did not suggest severe inflammation, as only focal aggregates of inflammatory cells were observed (near blood vessels, terminal ducts) and there was no evidence of fibrotic changes, giant cells, or granulomatous reactions. These data and those presented in Table VII suggest that the damage could be reversible at or below the exposure concentration used in the 5 m exposures (100 μg/m^3).

Since in vitro studies demonstrate that the production of Mip-2 and Ccl2 are strongly mediated by the presence of Tnf-α and Il-1α (Barlow et al., 2005; Driscoll et al., 1997; O'Brien et al., 1998), these cytokines were assessed in lung tissue as well. Tnf-α mRNA expression was significantly up-regulated in lungs acutely exposed to the high exposure concentration and repeatedly exposed for 3 m (Figure 7). And an increase in Il-1α expression was only detected following 5m of exposure to 100 μg/m^3 of nano-$Ni(OH)_2$ (Figure 7B). The lack of significance observed for Il-1α and Tnf-α at other concentrations in our study was interesting, given the potent nature of these cytokines in the progression of inflammatory events. It is possible that the observed response is related to the dynamic nature of the cytokine network, especially in a repeated, long-term exposure scenario.

In conclusion, we have shown that short and long-term inhalation exposures to nano-$Ni(OH)_2$ at occupationally relevant doses are capable of inducing inflammatory responses in

the lungs. We observed significant leukocyte influxes; increases in total and specific protein concentrations in BALF, altered mRNA expression for inflammatory related cytokines and chemokines, and histological evidence of mild inflammation. While the physicochemical properties which modulate these toxic events are still largely unknown, we speculate that the observed biological responses were due to the presence of both dissolved nickel ions and nanosized particles given the deposition, clearance, and dissolution data for nano-$Ni(OH)_2$ measured in acute studies and the accumulation of nickel measured in longer term studies. Since distinct mechanisms of toxicity are associated with nickel ions and nanosized particles, we have performed additional exposures with nickel sulfate hexahydrate in an effort to distinguish effects of soluble ion vs. less rapidly soluble nano-$Ni(OH)_2$ NPs (manuscript in preparation). Additional research is warranted to further investigate effects of inhaled nano-$Ni(OH)_2$, since these particles are under-studied and highly favorable for use as a chemical energy source in power/energy markets, placing occupational populations at risk.

Acknowledgments

The authors would like to thank Mr Mianhua Zhong for assistance in setting up the exposure system; Mr Alan Bowers for analyzing tissue samples with the GFAAS; and Dr Alice Liang and Mr Eric W. Roth from NYU School of Medicine Image Core Facility for assistance with TEM analyses. In addition, the authors graciously thank Ms Deborah Andrews, Ms Mette Schladweiler, and Dr Urmila Kodavanti of the U.S. Environmental Protection Agency for performing NAG and MCP-1 analyses.

This research was supported by the National Institutes of Health (RO1 ES015439 to L.C.; RO1 CA134218 to A.E.; P30 ESO1247, and ESO0260); and the Environmental Protection Agency (STAR Grant RD-8325280 to T.G.).

References

Bakand S, Winder C, Khalil C, Hayes A. Toxicity Assessment of Industrial Chemicals and Airborne Contaminants: Transition from *In Vivo* to *In Vitro* Test Methods: A Review. Inhal. Toxicol 2005;17:775–787. [PubMed: 16195213]

Barlow PG, Clouter-Baker A, Donaldson K, MacCallum J, Stone V. Carbon black nanoparticles induce type II epithelial cells to release chemotaxins for alveolar macrophages. Part. Fibre Toxicol 2005;2:11. [PubMed: 16332254]

Benson JM, Henderson RF, McClellan RO, Hanson RL, Rebar AH. Comparative Acute Toxicity of Four Nickel Compounds to F344 Rat Lung. Fund. Appl. Tox 1986;7:340–347.

Benson JM, Chang IY, Cheng YS, Hahn FF, Kennedy CH, Barr EB, Maples KR, Snipes MB. Particle clearance and histopathology in lungs of F344/N rats and $B6C3F_1$ mice inhaling nickel oxide or nickel sulfate. Fundam Appl. Toxicol 1995;28:232–244. [PubMed: 8835233]

Bernstein, SE. Physiological Characteristics. In: Green, EL., editor. Biology of the Laboratory Mouse. 2nd ed.. New York: Dover; 1975. p. 337-350.

Boyer JM, Répetti B, Garrigos R, Meyer M, Bée A. Thermal behavior of nickel hydroxide nanopowders. J. Metastable Nanocryst Mater 2004;22:1–11.

Chen LC, Schlesinger RB. Response of the bronchial mucociliary clearance system in rabbits to inhaled sulfite and sulfuric acid aerosols. Toxicol. Appl. Pharmacol 1983;71:123–131. [PubMed: 6636178]

Chen H, Davidson T, Singleton S, Garrick MD, Costa M. Nickel decreases cellular iron level and converts cytosolic aconitase to iron-regulatory protein 1 in A549 cells. Toxicol. Appl. Pharmacol 2005;206(3):275–287. [PubMed: 16039939]

Davidson T, Chen H, Garrick MD, D'Angelo G, Costa M. Soluble nickel interferes with cellular iron homeostasis. Mol. Cell. Biochem 2005;279:157–162. [PubMed: 16283525]

Donaldson K, Stone V. Current hypotheses on the mechanisms of toxicity of ultrafine particles. Ann. 1st Super Sanità 2003;39:405–410.

Dorato MA. Overview of Inhalation Toxicology. Environ. Health Perspect 1990;85:163–170. [PubMed: 2200660]

Driscoll KE, Carter JM, Hassenbein DG, Howard B. Cytokines and Particle-induced Inflammatory Cell Recruitment. Environ. Health Perspect 1997;105:1159–1164. [PubMed: 9400717]

Driscoll KE, Hassenbein DG, Howard BW, Isfort RJ, Cody D, Tindal MH, Suchanek M, Carter JM. Cloning, expression, and functional characterization of rat MIP-2: A neutrophil chemoattractant and epithelial cell mitogen. Leukoc Biol 1995;58:359–364.

Elder A, Gelein R, Silva V, Feikert T, Opanashuk L, Carter J, Potter R, Maynard A, Ito Y, Finkelstein J, Oberdörster G. Translocation of inhaled ultrafine manganese oxide particles to the central nervous system. Environ. Health Perspect 2006;114:1172–1178. [PubMed: 16882521]

Fahey TJ III, Tracey KJ, Tekamp-Olson P, Cousens LS, Jones WG, Shires GT, Cerami A, Sherry B. Macrophage inflammatory protein 1 modulates macrophage function. J Immunol 1992;148:2764–2769. [PubMed: 1573267]

Fangli Y, Peng H, Chunlei Y, Shulan H, Jinlin L. Preparation and properties of zinc oxide nanoparticles coated with zinc aluminate. J. Mater. Chem 2003;13:634–637.

Feghali CA, Wright TM. Cytokines in Acute and Chronic Inflammation. Front. Biosci 1997;2:d12–d26. [PubMed: 9159205]

Fetcenko MA, Ovshinsky SR, Reichman B, Young K, Fierro C, Koch J, Zallen A, Mays W, Ouchi T. Recent advances in NiMH battery technology. J. Power Sources 2007;165:544–551.

Fletcher GG, Rossetto FE, Turnbull JD, Nieboer E. Toxicity, Uptake, and Mutagenicity of Particulate and Soluble Nickel Compounds. Environ. Health Perspect 1994;102:69–79. [PubMed: 7843140]

Fulton SA, Reba SM, Martin TD, Boom WH. Neutrophil- Mediated Mycobacteriocidal Immunity in the Lung during *Mycobacterium bovis* BCG Infection in C57BL/6 Mice. Infect Immun 2002;70(9):5322–5327. [PubMed: 12183593]

Geiser M, Casaulta M, Kupferschmid B, Schulz H, Semmler-Behnke M, Kreyling W. The role of macrophages in the clearance of inhaled ultrafine titanium dioxide particles. Am. J. Respir. Cell Mol. Biol 2008;38:371–376. [PubMed: 17947511]

Gojova A, Guo B, Kota RS, Rutledge JC, Kennedy IM, Barakat AI. Induction of inflammation in vascular endothelial cells by metal oxide nanoparticles: effect of particle composition. Environ Health Perspect 2007;115(3):403–409. [PubMed: 17431490]

Gornostaeva SV, Revina AA, Belyakova LD, Larionov OG. Synthesis and Properties of Nickel Nanoparticles and Their Nanocomposites. Protection of Metals 2008;44:372–375.

Hammond RB, Pencheva K, Roberts KJ, Auffret T. Quantifying Solubility Enhancement Due to Particle Size Reduction and Crystal Habit Modification: Case Study of Acetyl Salicylic Acid. J. Pharm. Sci 2007;96:1967–1973. [PubMed: 17323349]

Hofmann W, Asgharian B. The Effect of Lung Structure on Mucociliary Clearance and Particle Retention in Human and Rat Lungs. Toxicol. Sci 2003;73:448–456. [PubMed: 12700392]

Hsieh TH, Yu CP, Oberdörster G. Deposition and Clearance Models of *Ni* Compounds in the Mouse Lung and Comparisons with the Rat Models. Aerosol Sci. Tech 1999;31:358–372.

International Commission on Radiological Protection (ICRP). Annals of the ICRP. Vol. 24. Oxford: Elsevier Science; 1994. Human Respiratory Tract Model for Radiological Protection; p. 1-300.

Kasprzak KS, Gabryel P, Jarczewska K. Carcinogenicity of nickel(II)hydroxides and nickel(II)sulfate in Wistar rats and its relation to the *in vitro* dissolution rates. Carcinogensis 1983;4:275–279.

Ke Q, Davidson T, Kluz T, Oller A, Costa M. Fluorescent tracking of nickel ions in human cultured cells. Toxicol. Appl. Pharmacol 2007;219:18–23. [PubMed: 17239912]

Lewinski N, Colvin V, Drezek R. Cytotoxicity of nanoparticles. Small 2008;4:26–49. [PubMed: 18165959]

Li CP, Proctor A, Hercules DM. Curve Fitting Analysis of ESCA Ni 2p Spectra of Nickel-Oxygen Compounds and Ni/Al_2O_3 Catalysts. Appl. Spectrosc 1984;38:880–886.

Lu H, Shi X, Costa M, Huang C. Carcinogenic effect of nickel compounds. Mol Cell Biochem 2005;279(1–2):45–67. [PubMed: 16283514]

Maciejczyk P, Zhong M, Li Q, Xiong J, Nadziejko C, Chen LC. Effects of subchronic exposures to concentrated ambient particles (CAPs) in mice. II. The design of a CAPs exposure system for biometric telemetry monitoring. Inhal. Toxicol 2005;17:189–197. [PubMed: 15804936]

Maus UA, Waelsch K, Kuziel WA, Delbeck T, Mack M, Blackwell TS, Christman JW, Schlondorff D, Seeger W, Lohmeyer J. Monocytes are potent facilitators of alveolar neutrophil emigration during lung inflammation: role of the CCL2-CCR2 axis. J Immunol 2003;170:3273–3278. [PubMed: 12626586]

Maynard AD. Nanotechnology: the next big thing, or much ado about nothing? Ann. Occup. Hyg 2007;51:1–12. [PubMed: 17041243]

Oberdörster G, Ferin J, Lehnert BE. Correlation between Particle Size, *In Vivo* Particle Persistence, and Lung Injury. Environ. Health Perspect 1994;102:173–179.

O'Brien AD, Standiford TJ, Christensen PJ, Wilcoxen SE, Paine R III. Chemotaxis of alveolar macrophages in response to signals derived from alveolar epithelial cells. J.Lab. Clin. Med 1998;131:417–424. [PubMed: 9605106]

Oller A. Respiratory Carcinogenicity Assessment of Soluble Nickel Compounds. Environ. Health Prespect 2002;110:841–844.

Pettibone JM, Adamcakova-Dodd A, Thorne PS, O'Shaughnessy PT, Weydert JA, Grassian VH. Nanotoxicology 2008;2(4):189–204.

Potter RM, Mattson SM. Glass fiber dissolution in a physiological saline solution. Glastech. Ber 1991;84:16–28.

Roco, MC.; Bainbridge, W. Societal Implications of Nanoscience and Nanotechnology. Boston: Springer; 2001. p. 1-350.

van Ravenzwaay B, Landsiedel R, Fabian E, Burkhardt S, Strauss V, Ma-Hock L. Comparing fate and effects of three particles of different surface properties: nano-TiO(2), pigmentary TiO(2) and quartz. Toxicol Lett 2009;186(3):152–159. [PubMed: 19114093]

Schlesinger RB. Effects of Inhaled Acids on Respiratory Tract Defense Mechanisms. Environ. Health Perspect 1985;63:25–38. [PubMed: 3908089]

Sergeev, GB. Nanochemistry. 1st ed.. Oxford: Elsevier Science; 2006. Size Effects in Nanochemistry; p. 170-172.

Venkatachari P, Hopke P, Grover B, Eatough D. Measurement of particle-based reactive oxygen species in Rubidoux aerosols. J. Atmo. Chem 2005;50:49–58.

Vidotti M, Silva MR, Salvador RP, Córdoba de Torresi SI, Dall'Antonia LH. Electrocatalytic oxidation of urea by nanostructured nickel/cobalt hydroxide electrodes. Electrochimica Acta 2008;53:4030–4034.

Xiao-yan G, Jian-cheng D. Preparation and electrochemical performance of nano-scale nickel hydroxide with different shapes. Mater. Lett 2007;61:621–625.

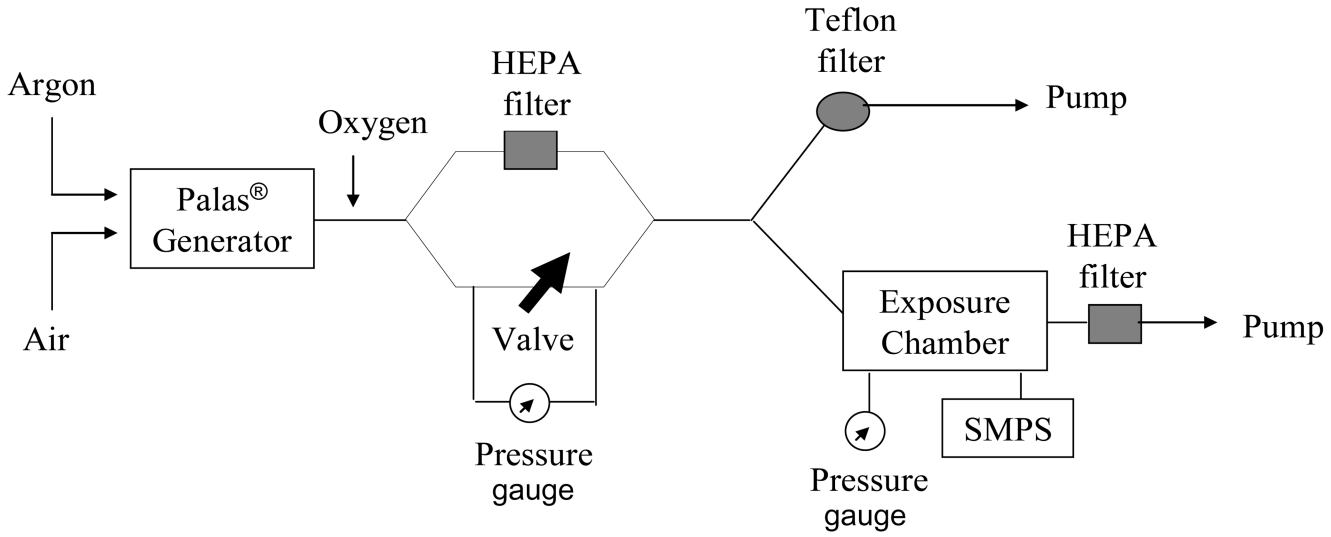

Figure 1.
A schematic diagram of the exposure system for nano-$Ni(OH)_2$ generation.

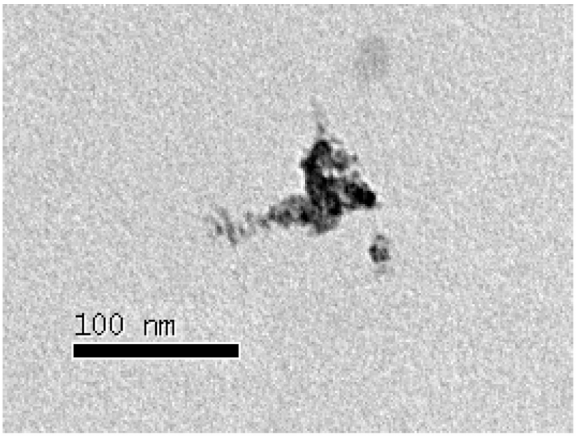

Figure 2A.

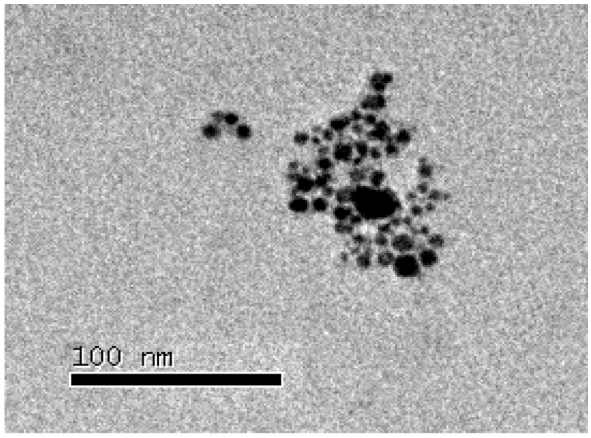

Figure 2B.

Figure 2.

TEM micrographs of nano-$Ni(OH)_2$ captured on 0.5% formvar covered carbon grids. (A) 110k magnification image of nano-$Ni(OH)_2$ collected from the Palas® generator. (B) 140k magnification image of nano-$Ni(OH)_2$ found 0.5h post-exposure in lavage fluid collected from a mouse exposed to the high concentration. Scale bars are included.

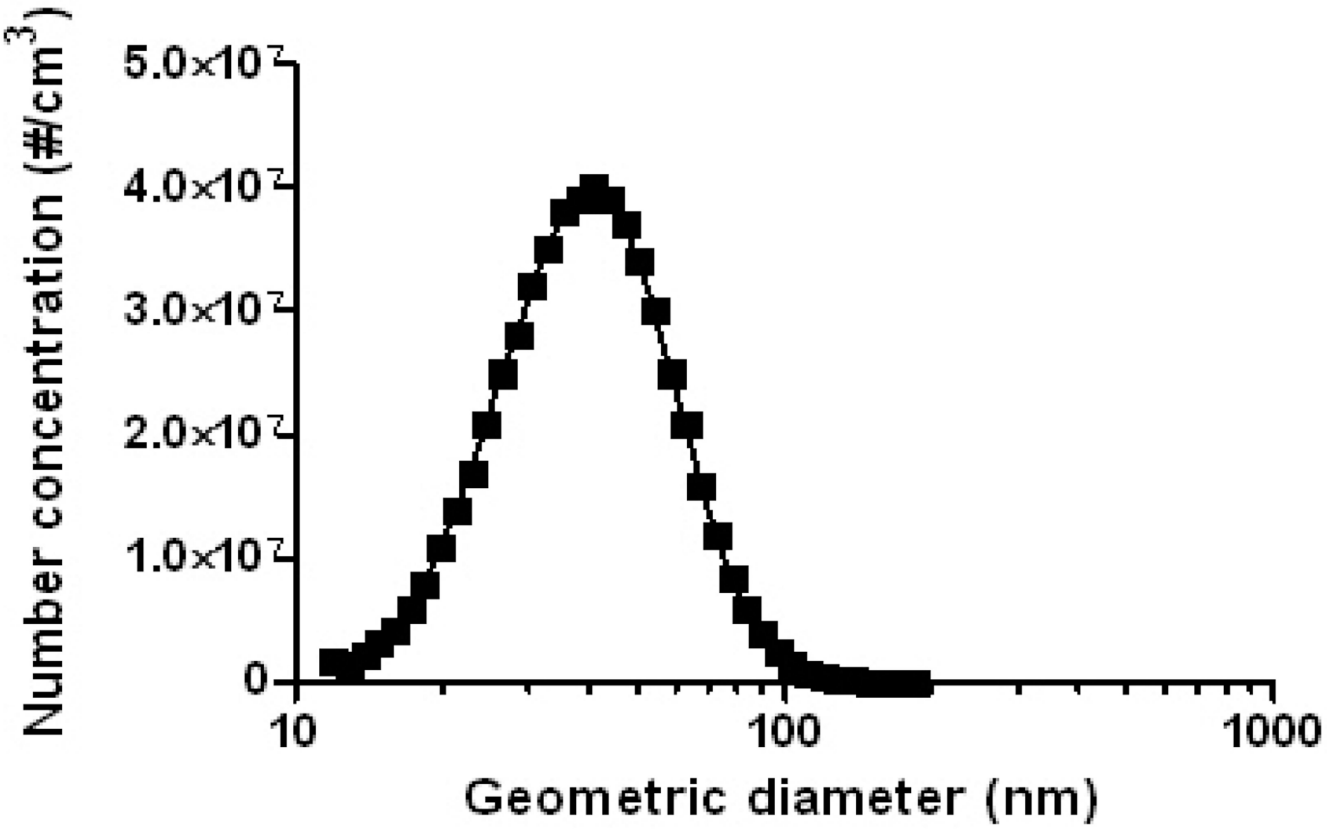

Figure 3.
A representative size distribution of nano-$Ni(OH)_2$ monitored by SMPS. Particle size distributions were the same for all three tested nominal concentrations (100, 500, and 1000 $\mu g/m^3$).

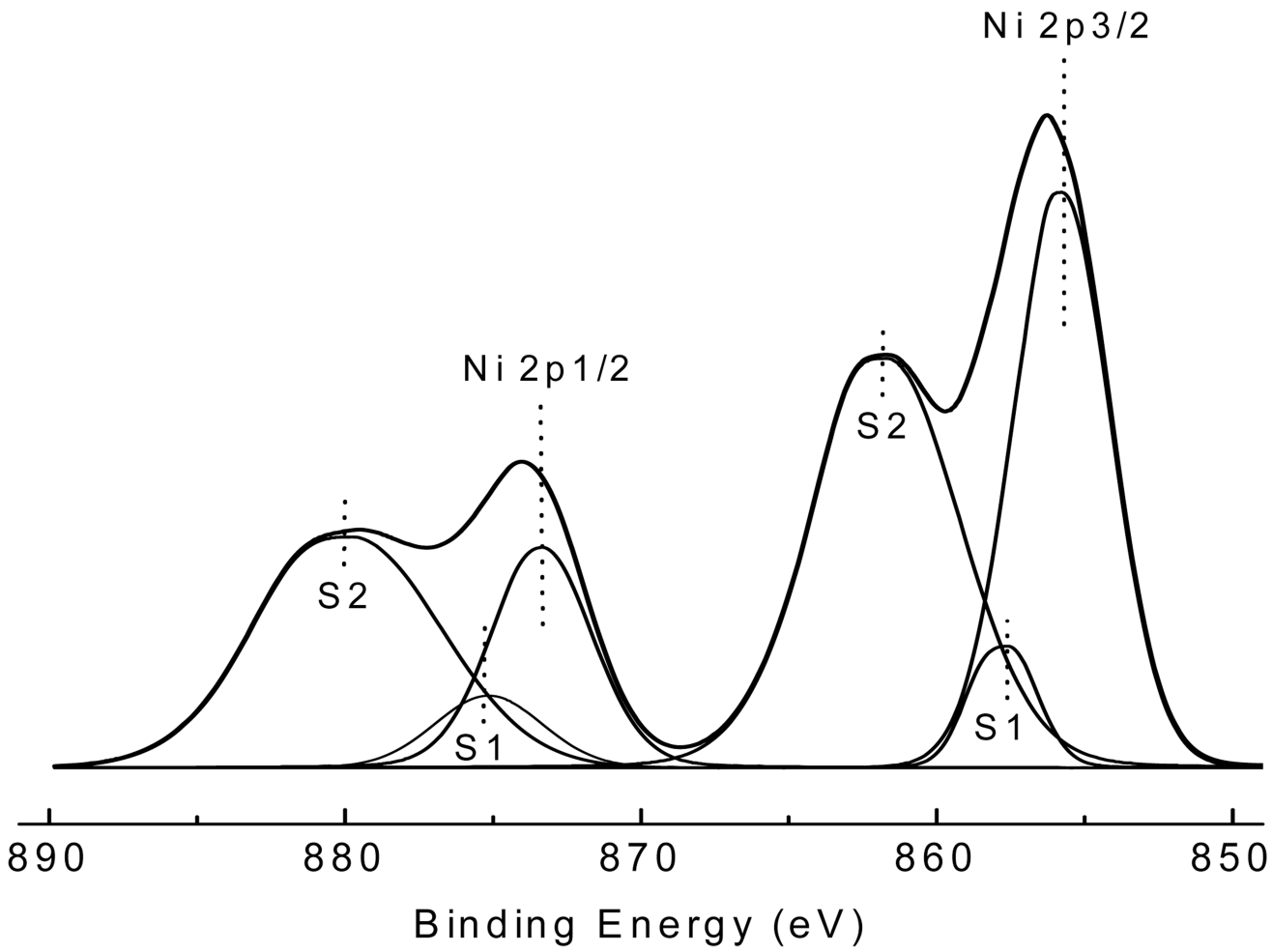

Figure 4.
Curve fitting of the Ni 2p spectrum from generated nano-$Ni(OH)_2$. In the Ni 2p region, there are two main peaks 2p3/2 and 2p1/2; for each main peak, there are two shake-up satellite peaks S1 and S2. The peak positions and area percentages are shown in Table II.

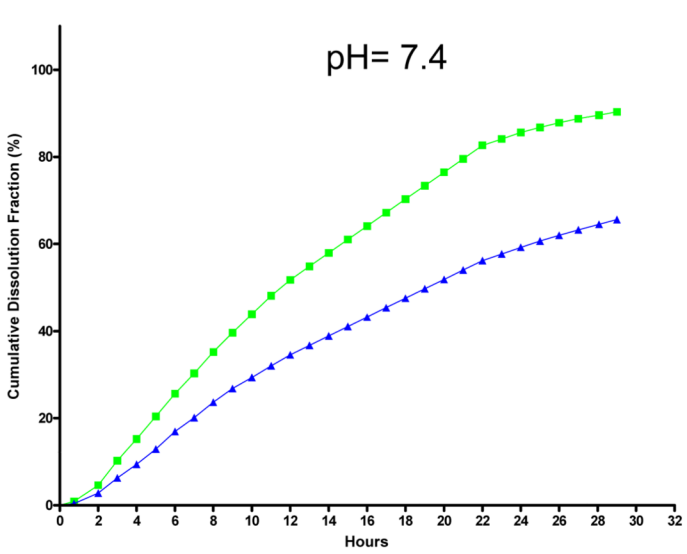

Figure 5A.

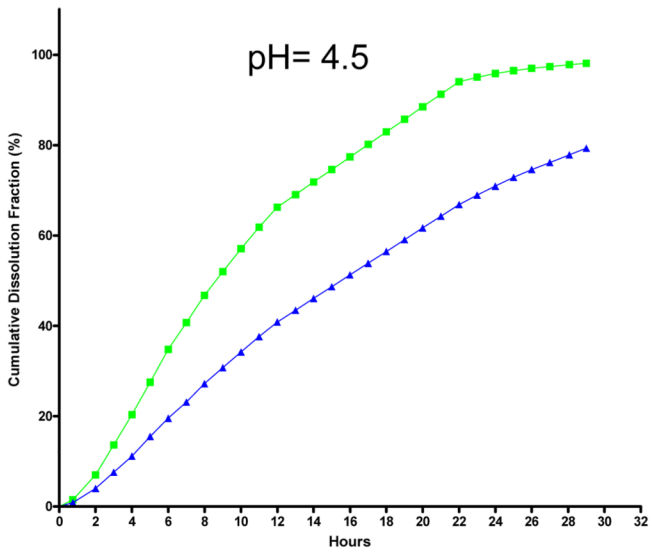

Figure 5B.

Figure 5.
Nano-$Ni(OH)_2$ dissolution rates in physiologic buffers systems at (A) pH 7.4 or (B) pH 4.5. Dissolution was measured at 37 °C (green squares) and room temperature (~23 °C, blue triangles).

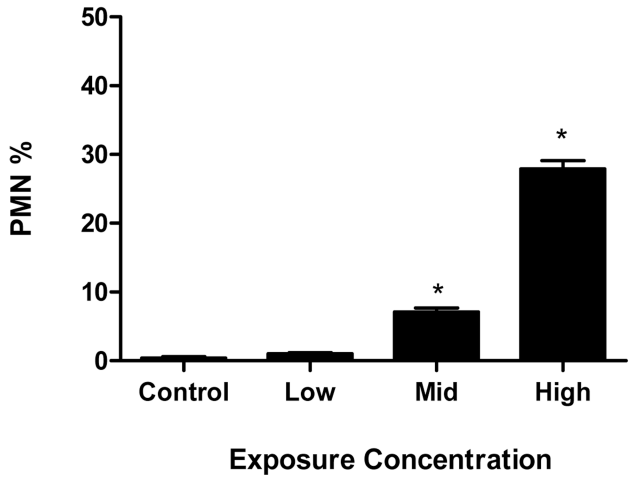

Figure 6A.

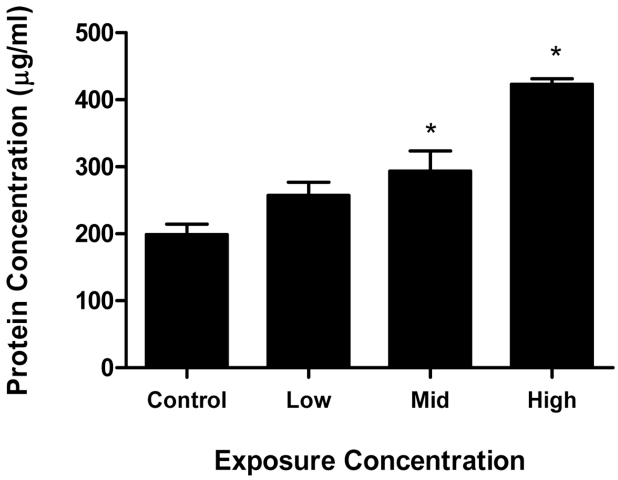

Figure 6B.

Figure 6.
BALF inflammatory markers: (A) polymorphonuclear leukocyte (PMN) percent and (B) total protein level at 24 h post-exposure (n = 3–4/group) for short term studies.

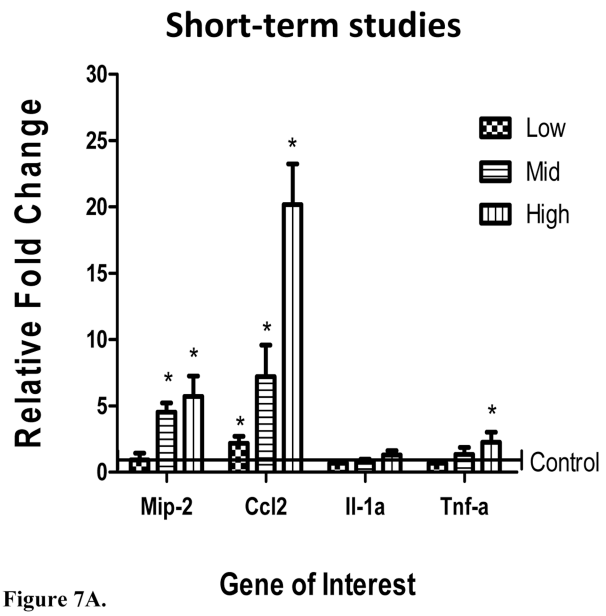

Figure 7A.

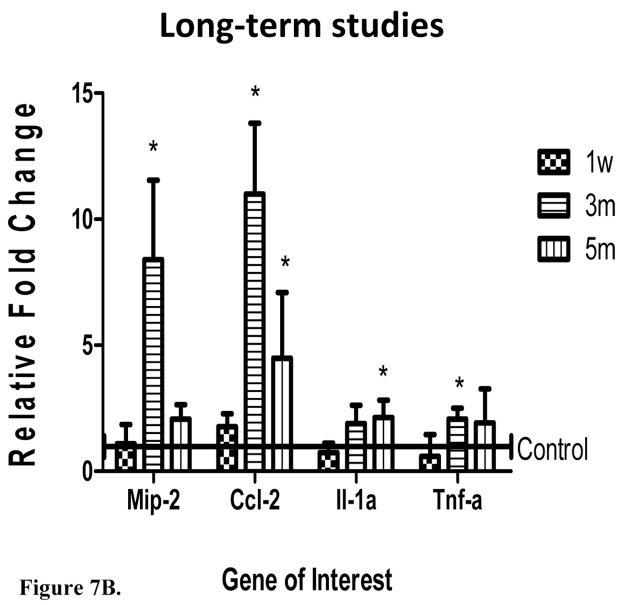

Figure 7B.

Figure 7.

mRNA expression of Mip-2, Ccl2, Il-1α, and Tnf-α in lavaged lung tissue of mice exposed to (A) low, mid, and high concentrations of nano-$Ni(OH)_2$ (n = 3–4/group) and (B) 1 w, 3 m and 5 m of exposure to nano-$Ni(OH)_2$ (n = 3–4/group). Concentrations for 1 w, 3 m, and 5 m exposures were 124.0, 129.3, and 124.5 μg/m^3 (78.6, 82.0, 79.0 μg Ni/m^3), respectively. Data are reported at 24 h post-exposure as a relative fold change over control (± SD) and asterisks indicate a statistically significant difference between nickel exposed and control groups as determined by student's t-test (*$P<0.05$).

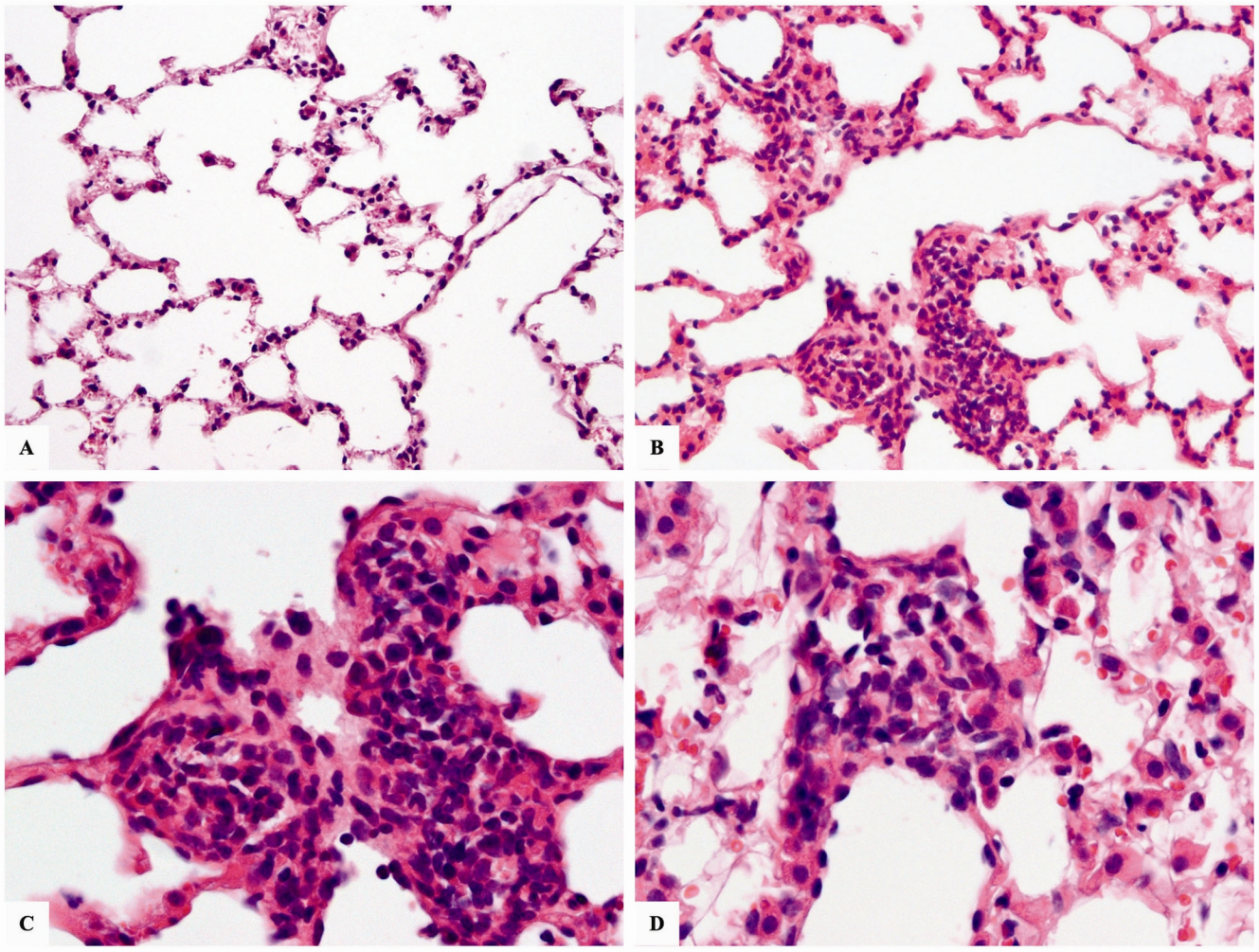

Figure 8.
Micrographs of representative H&E stained lung sections from mice exposed to 124.5 μg/m^3 (79.0 μg Ni/m3) of nano-$Ni(OH)_2$ for 5 m. (A) normal lung at 20×; (B) exposed mouse lung section showing chronic inflammatory infiltrate in a terminal duct at 20×; (C) same as previous, showing a predominance of lymphocytes at 40×; (D) inflammatory infiltrate in the pulmonary interstitial space of exposed mouse at 40×.

Table I

Summary of nickel hydroxide nanoparticles mass concentrations and size for all studies

Exposure Concentration Group	Low	Mid	High	1w	3m	5m
Nominal mass conc. (μg/m^3)	100	500	1000	100	100	100
Actual mass conc. (μg/m^3) [a]	103.2 ± 20.0 [b]	565.0 ± 7.1 [b]	1204.0 ± 25.7 [b]	124.0 ± 31.3	129.3 ± 9.36	124.5 ± 4.10
Nickel mass conc. (μg Ni/m^3) [a]	65.4 ± 12.7	358.2 ± 4.5	763.3 ± 16.3	78.6 ± 19.9	82.0 ± 5.93	79.0 ± 2.60
Number conc. (#/cm^3) [c]	2.3 E+06	1.8 E+07	2.8 E+07	—	—	—
Count Median Diameter (CMD, nm) [c]	40.1	38.4	39.1	—	—	—
Geometric Standard Deviation (GSD) [c]	1.57	1.49	1.45	—	—	—
Surface area (m^2/g)[d]	36.1	37.7	37.0			

Abbreviations: conc, concentration; #, total number of particles;

[a] Values are the average of two measurements ± SD,

[b] Values represents mean ± SEM,

[c] Data not shown for long-term studies however values agreed well with those determined for the low exposure short term studies.

[d] Values were calculated based on particle size. Functional surface measurements were not performed.

Table II

Peak positions and area percentages of nickel 2p lines from curve fitting (see Figure 4)

	Ni 2p3/2			Ni 2p1/2		
	Main peak	**S1**	**S2**	**Main peak**	**S1**	**S2**
Peak position (eV)	855.8	857.6	861.7	873.4	875.2	879.8
Area %	28	4.2	31.1	11.6	4.0	21.2

Table III

X-ray photoelectron spectroscopy parameters of nickel 2p satellite lines for various nickel compounds

	Ni 2p3/2				Ni 2p1/2			
	S1 Satellite		S2 Satellite		S1 Satellite		S2 Satellite	
	ΔE_{sat}	I_s/I_m	ΔE_{sat}	I_s/I_m	ΔE_{sat}	I_s/I_m	ΔE_{sat}	I_s/I_m
Ni metal [a]	—	—	5.8	0.174	—	—	4.4	0.391
NiO [a]	1.9	1.165	6.5	1.864	1.9	1.383	7.4	3.933
$Ni(OH)_2$ [a]	1.8	0.115	5.8	1.049	1.8	0.353	6.3	1.825
Generated Particles	1.8	0.150	5.9	1.111	1.8	0.345	6.4	1.828

[a] Reported in literature (Li et al., 1984).

Table IV

Cell-free reactive oxygen species generation by nickel hydroxide nanoparticles and soluble nickel.

Nickel (μg)	Nano-$Ni(OH)_2$ H_2O_2 equivalents (nM)	$NiSO_4 \cdot 6H_2O$ H_2O_2 equivalents (nM)
0.16	98	<LLD
0.32	193	<LLD
0.63	408	<LLD
1.59	970	25
3.16	1760	21
6.32	3172	<LLD

Data are expressed as H_2O_2 equivalents.

Abbreviations: <LLD, below the lower limit of detection.

Table V

Summary of nickel content in lungs after short-term exposures to nickel hydroxide nanoparticles.

Exposure Group	Ni content- 0.5 h PE (ng Ni/g of tissue)	Ni content- 24 h PE (ng Ni/g of tissue)	Ni content- 48 h PE (ng Ni/g of tissue)
Control	—	8.95 ± 5.15	—
Low	285.8 ± 47.03*	86.1 ± 26.5*	60.7± 8.82*
Mid	2200.0 ± 146.6*	1210.0 ± 169.2*	ND
High	4200.3 ± 384.3*	2270.0 ± 42.2*	1538.5 ± 17.5*

Abbreviations: PE, post-exposure; ND, not determined.

Reported values are averages of individually measured lung samples ± SEM; n = 3–4 for Ni-exposed mice and n = 3 for controls.

Asterisks indicate a statistically significant difference between nickel exposed and control groups (*P<0.05).

Table VI

Summary of nickel content in lungs after long-term studies to nickel hydroxide nanoparticles.

Exposure Duration	Ni content- 24 h PE (ng Ni/g of tissue)
Control	17.9 ± 9.74
1w	147.8 ± 7.96*
3m	558.8 ± 1.31*
5m	925.2 ± 27.7*

Abbreviations: PE, post-exposure.

Reported values are averages of individually measured lung samples (n=3–4 for Ni-exposed mice and n=3 for controls).

Asterisks indicate a statistically significant difference between nickel exposed and control groups (*P<0.05).

Concentrations for 1 w, 3 m, and 5 m exposures were 124.0, 129.3, and 124.5 μg/m^3 (78.6, 82.0, 79.0 μg Ni/m^3), respectively.

Table VII

Summary of bronchoalveolar lavage fluid data 24 h after long-term exposures to nickel hydroxide nanoparticles.

Biochemical Assay	Control	1w	3m	5m
Macrophage (%)	99.1 ± 0.52	95.9 ± 0.52	85.3 ± 0.88*	86.0 ± 2.57*
PMN (%)	0.63 ± 0.38	3.13 ± 0.63	9.50 ± 1.50*	6.17 ± 1.09*
Lymphocytes (%)	0.25 ± 0.25	0.50 ± 0.29	5.17 ± 0.73*	7.83 ± 1.86*
Total protein (mg/ml)	241.3 ± 11.95	282.2 ± 25.83	490.8 ± 26.64*	400.7 ± 42.91*
NAG (U/l)	6.41 ± 0.16	7.99 ± 0.38	ND	10.6 ± 1.26*
MCP-1 (μg/ml)	<LLD	<LLD	38.2 ± 5.70*	46.2 ± 11.1*

Abbreviations: PMN, polymorphonuclear leukocyte; NAG, N-acetyl-glucosaminidase; ND, not determined; <LLD; below lower limit of detection.

Reported values are mean ± SEM; n = 4 for Ni-exposed mice and n = 9 for controls.

Asterisks indicate a statistically significant difference between nickel exposed and control groups (*P<0.05).

Concentrations for 1 w, 3 m, and 5 m exposures were 124.0, 129.3, and 124.5 μg/m^3 (78.6, 82.0, 79.0 μg Ni/m^3), respectively.